ISSN 1392–1207. MECHANIKA. 2022 Volume 28(4): 283–293

Profile Design and Performance Research of Hydrogen Circulation Pump in Fuel Cell System

Huanle ZHAI*,, Wei LI*,***, Leilei JI*,****, Muhammad AWAIS*, Jiwei LI**, Shuo LI***

**National Research Center of Pumps, Jiangsu University, Zhenjiang 212013, China, E-mail: lwjiangda@ujs.edu.cn*
***Aviation Engineering Institute, Jiangsu Aviation Technical College, 212134, China, E-mail: jszhaihl@163.com*
****Institute of Fluid Engineering Equipment Technology, Jiangsu University, Zhenjiang 212009, China, E-mail: lwjiangda@ujs.edu.cn*
*****Wenling Fluid Machinery Technology Institute of Jiangsu University, Wenling 317525, China, E-mail: leileiji@ujs.edu.cn*

crossref http://dx.doi.org/10.5755/j02.mech.31528

Nomenclature

L – the length of the pump cavity; B – the width of the pump cavity; D – the height of the pump cavity; R_m – the tip radius of the rotor profile; R – the pitch radius of the rotor profile; δ_1 – the gap between rotor and pump casing; δ_2 – the gap between the two rotors; n – the number of rotor blades; α – the envelope angle of the curve I; P_d – the outlet pressure of the hydrogen circulating pump; P_s – the inlet pressure of the hydrogen circulating pump; Q_d – the outlet flow rate of the hydrogen circulating pump;

Abbreviation

HCP – hydrogen circulating pump; P Tra. – pressure transmitter; T Tra. – temperature transmitter; MF – mass flowmeter.

1. Introduction

Fuel cell technology can meet the needs of society for clean energy and renewable energy with excellent development prospects [1-2]. During the working process of the fuel cell system, the high content of water generated by the combination of hydrogen ions and oxygen ions will hinder the gas diffusion, resulting in a decrease in the output voltage of the stack. The accumulation of impurity gas penetrating from the cathode side to the anode will also affect the performance and life span of the stack. For the problems of water blocking and gas permeation, the cathode discharge method is usually used to discharge the generated water and accumulated impurity gas inside the stack. However, if the discharge frequency is too low, it is easy to cause water blockage and accumulation of impurity gas, which will lead to the decline of the stack's performance. If the discharge frequency is too high, a large amount of hydrogen will be discharged, which wastes hydrogen and brings potential dangers [3-5]. Therefore, it is necessary to use hydrogen recycling equipment to recover unconsumed hydrogen from the anode and transport it back to the stack inlet to improve the hydrogen utilization efficiency and optimize the life and performance of the fuel cell stack, as shown in Fig. 1.

Hydrogen recirculation equipment mainly includes two types, ejector and mechanical pump. The recirculation equipment can be used individually or in parallel. The ejector uses the pressure difference between the hydrogen tank and the fuel cell stack as the driving force. It has the advantages of the low maintenance cost, no moving parts, and the efficiency is relatively high [6-7]. The disadvantage is that when the fuel cell on and off or changes the load, its working stability is difficult to guarantee, especially in the low power region [8]. According to their structure, mechanical pumps can be divided into claw pumps, roots pumps, and scroll pumps. The claw pump is a rotary positive displacement pump with built-in compression, which has the advantages of a compact and straightforward structure [9]. However, its disadvantage of large fluctuations in output pressure and flow [10]. The scroll pump works through the meshing of two scrolls with close clearance, which has the advantages of high efficiency, wide adjustable range of flow, low noise, and small vibration [11-12]. However, due to their low operating rates, scroll pumps have lower flow rates than comparably sized Roots or claw pumps and are therefore only suitable for micro or small systems [13]. The Roots pump is also a rotary positive displacement pump, which carries gas by rotating a pair of rotors with cogging grooves. It has the advantages of simple structure, high reliability, low cost, suitable for large flow, and has the disadvantage of low efficiency [14]. Since high reliability, large flow, and low cost are more essentialfactors in practical applications. Therefore. the Roots pump structure is a good choice for the fuel cell hydrogen recirculation systemand has been used in the fuel cell vehicle field. Feng Jianmei [15] studied the performance of the Roots hydrogen pump with a three-blade helical rotor structure through extensive simulations and experimental verification. They found that the volumetric efficiency and isentropic efficiency were improved with the increased fraction of water vapor and nitrogen. Jiawei Lin [16] designed an efficient and reasonable rotor profile for the Roots hydrogen pump, used the motion simulation module in UG NX to conduct a simulation analysis of rotor mechanism meshing motion on the rotating parts, and obtained the angular velocity curve and meshing force change curve of the driven gear. Xing Linfen [17] has proved through experiments that the effect of the pressure difference on the flow rate and volumetric efficiency of the Roots pump is the most significant. The leakage has a major influence on volumetric isentropic efficiency.

The above literature is only for performance analysis of Roots hydrogen pumps with several conventional profiles, and no in-depth research on profile design theory. Profile design is the basis of Roots hydrogen pump design, which impacts volumetric efficiency, leakage rate, running stability, etc. It hasessentialresearch significance. Considering that the Roots structure is widely used in vacuum pumps, fans, and other fields, related profile design research results

can be used as a reference. For the involute rotor profile, although reducing the pressure angle reduces the area utilization factor, it increases the degree of coincidence and improves the stability and bearing capacity of the rotor transmission [18]. The two-tangent-arcs rotor profile also hasa high area utilization coefficient, and uniform meshing gap and isnot easy to leak [19]. Inserting a high-order curve between the involute and the arc can effectively eliminate the cusp phenomenon, thereby improving the "pulsation" at the output [20]. Multi-compound ellipse-involute-ellipse and corresponding conjugate curves have a higher volume utilization rate and improve hydraulic oil delivery efficiency [21]. Zhang Tiezhu and Zhang Hongxinet al. [22-23] used the rotor shape parameter as a variable to achieve the objective design of minimizing the cavity volume under the constraint of the cavity structure strength. Chiu-Fan et al. [24] established the profile by the trajectory of the long axis endpoint of the elliptical roller rolling around the arc, and obtained the relationship between the ellipse axis ratio parameter and the flow characteristics. Yan Jia et al. [25] used the deviation function method to correct the involute rotor profile to achieve the effect of high sealing and high efficiency.

Based on the previous research, this paper proposes the general design formula of the rotor profile of the hydrogen circulating pump, which can realize the design of various types of shapes. Then the calculation method based on the overset mesh and the realizable k-epsilon two-layer turbulence model is determined, and experiments verify its reliability. Finally, the performance differences of two-phase tangent arc type, single-arc type, ellipse type, and quadratic-curve type are analyzed to determine the optimal profile.

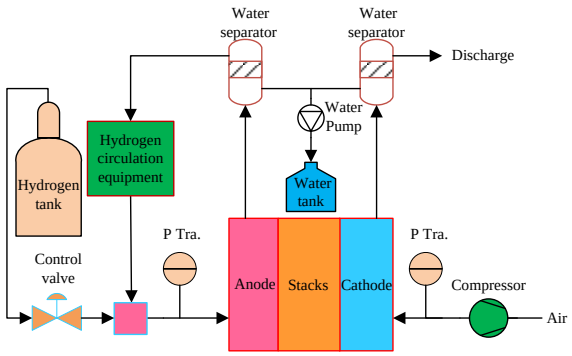

Fig. 1 Supply system of hydrogen fuel cell

2. Rotor profile design method

2.1. Conjugation theory

As shown in Fig. 2, the curve *I* rotates clockwise around the origin O_1. The curve *II* is the conjugate curve *I* and rotates counter clockwise around the origin O_2 with the same angular velocity. When the rotation angle is θ, the curve *I* and the curve *II* are tangent at point *M*, with the normals passing through this point intersecting the line O_1 O_2 at point *O*.

At point *M*, the running speeds of curve *I* and curve *II* are v_{MN_1} and v_{MN_2} respectively. Only when the components of the two running speeds on the normals *OM* are equal can the two curves be tangent at point *M*.

$$v_{MN_1} \times cos\angle NMN_1 = v_{MN_2} \times cos\angle NMN_2. \tag{1}$$

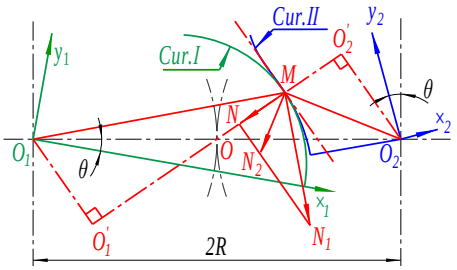

Fig. 2 Conjugate curve meshing principle

According to the angular velocity values of the curve *I* and the curve *II* being equal, it can be deduced that the distance O_1O_1' is equal to the distance O_2O_2'.

$$d_{O_1O_1'} = d_{O_1M} \times cos\angle MO_1O_1' = d_{O_2M} \times \\ \times cos\angle MO_2O_2' = d_{O_2O_2'}. \tag{2}$$

It follows that point *O* is the midpoint of the line O_1 O_2.

$$d_{O_1O} = d_{O_2O} = R. \tag{3}$$

Therefore, when the curve *I* and its conjugate curve *II* are in rotational meshing, the connection between the meshing point and the midpoint of the line O_1 O_2 is the common normals of the two curves at the meshing point.

2.2. Theoretical profile design method

To solve the conjugate curve *II* from the curve *I*, denote the equation of curve *I* in the moving coordinate system $x_1O_1y_1$ as $\boldsymbol{L}_1$, and the equation of curve *II* in the moving coordinate system $x_2O_2y_2$ as $\boldsymbol{L}_2$.

As the rotation angle θ changes, the trajectory of point *M* in the moving coordinate system $x_2O_2y_2$ forms the curve *II*. The coordinates of point M in the moving coordinate system $x_1O_1y_1$ can be transformed into the moving coordinate system $x_2O_2y_2$ through the coordinate transformation matrix $\boldsymbol{A}$.

$$\boldsymbol{L_i} = \begin{bmatrix} x_i(t) \\ y_i(t) \\ 1 \end{bmatrix} (i = 1, 2), \tag{4}$$

$$\frac{\partial y_1(t)}{\partial t} \times \frac{\partial t}{\partial x_1(t)} = \frac{Rcos\theta - x_1(t)}{y_1(t) - Rsin\theta}. \tag{5}$$

Under the rotation angle θ, according to the line *OM* is the normals of the curve *I* at the point *M*, it can be determined that the coordinates of the point M in the moving coordinate system $x_1O_1y_1$ satisfy Eq. (5).

Further derivation, we get:

$$cos\theta \frac{\partial x_1(t)}{\partial t} + sin\theta \frac{\partial y_1(t)}{\partial t} = \\ = \frac{1}{R}\left[y_1(t) \frac{\partial y_1(t)}{\partial t} + x_1(t) \frac{\partial x_1(t)}{\partial t} \right]. \tag{6}$$

Combined with formula (6), the equation $\boldsymbol{L}_2$ of the curve *II* in the moving coordinate system $x_2O_2y_2$ can be der-

ived.

$$\boldsymbol{A}=\begin{bmatrix} cos2\theta & sin2\theta & -2Rcos\theta \\ -sin2\theta & cos2\theta & 2Rsin\theta \\ 0 & 0 & 1 \end{bmatrix}, \tag{7}$$

$$\begin{cases} \boldsymbol{L_2}=\boldsymbol{AL_1}=\begin{bmatrix} x_1(t)cos2\theta+y_1(t)sin2\theta-2Rcos\theta \\ -x_1(t)sin2\theta+y_1(t)cos2\theta+2Rsin\theta \\ 1 \end{bmatrix} \\ \theta=\begin{cases} -arctan\dfrac{m}{n}+arcsin\dfrac{k}{\sqrt{m^2+n^2}}\left(n\geq 0\right) \\ \pi-arctan\dfrac{m}{n}+arcsin\dfrac{k}{\sqrt{m^2+n^2}}\left(n<0\right) \end{cases} \\ m=\dfrac{\partial x_1(t)}{\partial t} \\ n=\dfrac{\partial y_1(t)}{\partial t} \\ k=\dfrac{1}{R}\left[y_1(t)\dfrac{\partial y_1(t)}{\partial t}+x_1(t)\dfrac{\partial x_1(t)}{\partial t}\right] \end{cases}. \tag{8}$$

2.3. Actual profile design method

The formulas derived above are used for theoretical rotor profile design without considering the gap between components. However, in the actual profile design, to reduce friction, a certain gap must be developed between the rotorsor between the rotors and the pump casing. At the beginning of the design, the length L, width B of the pump cavity, the gap δ_1 between the rotors and the pump casing, and the gap δ_2 between the rotors should be defined first, as shown in Fig. 3.

From these known dimensions, determine the tip radius R_m and pitch radius R of the rotor profile.

$$R_m=\frac{B}{2}-\delta_1+\frac{\delta_2}{2}, \tag{9}$$

$$R=\frac{L-B}{2}. \tag{10}$$

Then according to the theoretical curve segment I, calculate the curve segment I_{rel} and II_{rel} of the actual rotor profile.

$$\begin{cases} \boldsymbol{L_{1rel}}=\boldsymbol{L_1}-\boldsymbol{\Gamma} \\ \boldsymbol{L_{2rel}}=\boldsymbol{A}\left(\boldsymbol{L_1}+\boldsymbol{\Gamma}\right) \\ \boldsymbol{\Gamma}=\begin{bmatrix} \dfrac{\delta_2 n}{2\sqrt{m^2+n^2}} \\ \dfrac{-\delta_2 m}{2\sqrt{m^2+n^2}} \\ 0 \end{bmatrix} \end{cases}. \tag{11}$$

3. Structural design and numerical simulation

3.1. Design conditions

Regarding the existing HCP product structure in the current market, the number of rotor blades and design conditionsare determined. The specific parameters are shown in Table 1.

Table 1

Design conditions

Parameters	Value
The length of the pump cavity L, mm	111
The width of the pump cavity B, mm	66
The height of the pump cavity D, mm	60
The gap between the rotor and the pump casing δ_1, mm	0.1
The gap between the two rotors δ_2, mm	0.1
Number of rotor blades n (envelope angle α)	2(π/4)

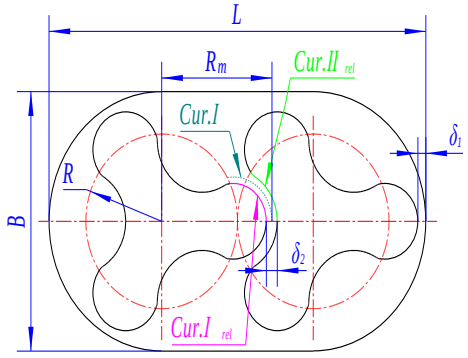

Fig. 3 Actual profile design

3.2. Designing process

The curve I of the rotor profile designed in this paper is composed of two-tangent-arcs, with the formula as follows:

$$\begin{cases} \boldsymbol{L_1}=\begin{cases} \begin{bmatrix} R_m-r_1+r_1cost \\ r_1sint \\ 1 \end{bmatrix} & \left(0\leq t<\gamma\right) \\ \begin{bmatrix} k_1+r_2cost \\ k_2+r_2sint \\ 1 \end{bmatrix} & \left(\gamma\leq t\leq \pi\text{-}arcsin\left(\dfrac{Rsin\alpha-k_2}{r_2}\right)\right) \end{cases} \\ k_1=R_m-r_1+r_1cos\gamma-r_2cos\gamma \\ k_2=r_1sin\gamma-r_2sin\gamma \\ r_2=\dfrac{\left(R_m-r_1+r_1cos\gamma-Rcos\alpha\right)^2+\left(Rsin\alpha-r_1sin\gamma\right)^2}{2\left[R_mcos\gamma-r_1cos\gamma+r_1-Rcos\left(\gamma-\alpha\right)\right]} \end{cases}. \tag{12}$$

In the formula, r_1 is the radius of the top arc, which is a variable parameter, and the value here is 32.9, that is the value of R_{mrel}; γ is the angle between the centerline of the top arc and the radial line of the tangent point, which is also a variable parameter, and the value here is $\pi/12$. Substitute $\boldsymbol{L}_1$ into formula (11), and then combine the corresponding relationship of each parameter in formula (8) to complete the calculation of the rotor profile formula. The final drawn rotor structure is shown in Fig. 4.

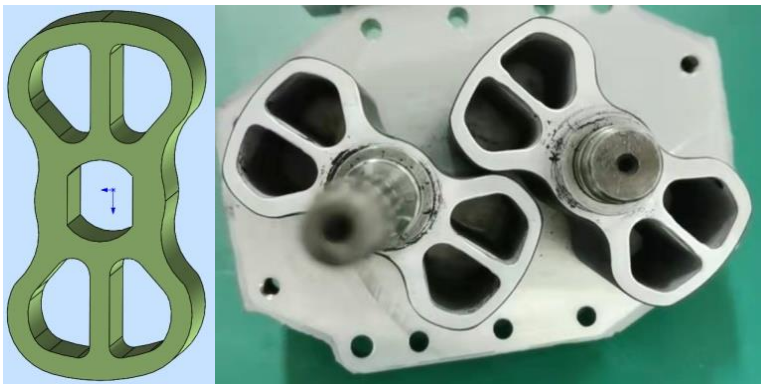

Fig. 4 Rotor structure

3.3. Numerical calculation method

3.3.1. Turbulence model

The turbulence model used in this paper is the realizable k-epsilon two-layer model, which combines the standard k-epsilon model with the two-layer method. This model is more suitable for low Reynolds number type meshes or wall function type meshes and can better simulate various flows in the whole flow field [26]. The main governing equations of the realizable k-epsilon two-layer turbulence model are shown in Eqs. (13) and (14), where the model coefficients $\sigma_k = 1$, $\sigma_\varepsilon = 1.2$, $C_{\varepsilon 1} = 1.44$, $C_{\varepsilon 2} = 1.9$.

3.3.2. Boundary conditions

According to the actual working state of the hydrogen circulating pump, set the inlet boundary type of the model as pressure inlet and the outlet boundary type as pressure outlet, and put all boundaries to 300K adiabatic condition.

$$\frac{\partial(\rho k)}{\partial t}+\nabla\cdot(\rho k\bar{v})=\nabla\cdot\left[\left(\mu+\frac{\mu_t}{\sigma_k}\right)\nabla k\right]+ +P_k-\rho(\varepsilon-\varepsilon_0)+S_k, \tag{13}$$

$$\frac{\partial(\rho\varepsilon)}{\partial t}+\nabla\cdot(\rho\varepsilon\bar{v})=\nabla\cdot\left[\left(\mu+\frac{\mu_t}{\sigma_\varepsilon}\right)\nabla\varepsilon\right]+ +\frac{1}{T_e}C_{\varepsilon 1}P_\varepsilon-C_{\varepsilon 2}f_2\rho\left(\frac{\varepsilon}{T_e}-\frac{\varepsilon_0}{T_0}\right)+S_\varepsilon. \tag{14}$$

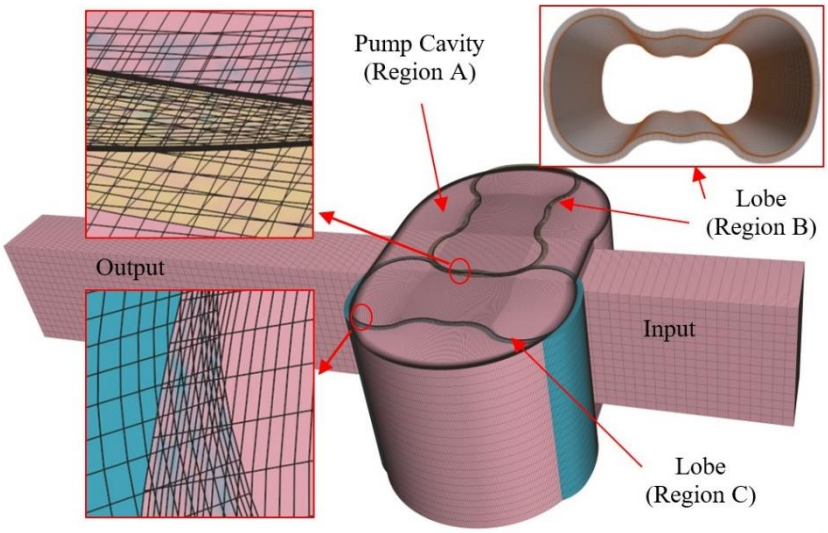

Fig 5 Grid model

3.3.3. Meshing

Considering that the relative motion gap is only 0.1 mm, this paper adopts the overset mesh method for simulation calculation. The overset mesh method couples the two regions by exchanging data between the acceptor grid cells in the background region and the donor grid cells in the overlapping region. The pump cavity is denoted as region A, and the two rotors extend a certain distance from the profile surface to be indicated as regions B and C, respectively. Three region couplings need to be set, namely A as the back-

ground region to couple with B and C, and B as the background region to couple with C. As shown in Fig. 5, the grid model of region A contains 2.0 million grids, the grid models of regions B and C include 0.4 million grids respectively, the inlet section contains 21 thousand grids. The outlet section contains 45 thousand grids. The STAR-CCM software is used for the simulation calculation of the mesh model. The software requires at least 4 element layers in the overlapping area to achieve accurate calculation. For the grid model in this paper, the number of element layers in the overlapping area of region A and region B/C at the motion gap is 5, and the number of element layers in the overlapping area of region B and region C at the motion gap is 6. The mesh density meets the precision calculation requirements of the STAR-CCM software.

4. Calculation results and experimental verification

4.1. Simulation results for different media

Set the running speed to 6000 rpm, the fluid medium to be hydrogen or air, and the pressure ratio P_d/P_s to be 1.1, 1.2, 1.3, and 1.4, respectively. According to the above method, the simulation calculation is carried out for the 8 working conditions of the model. The calculation results are shown in Fig 6. Under different pressure ratios, the average volume flow rate Q_d in the hydrogen medium is slightly lower than that in the air medium. The maximum error is 3.6 %, and the minimum is 0.8 %. The calculation results show that the Q_d of the hydrogen circulating pump model under the two media is similar, and the experimental and numerical comparison research can be carried out by replacing the hydrogen medium with the air medium.

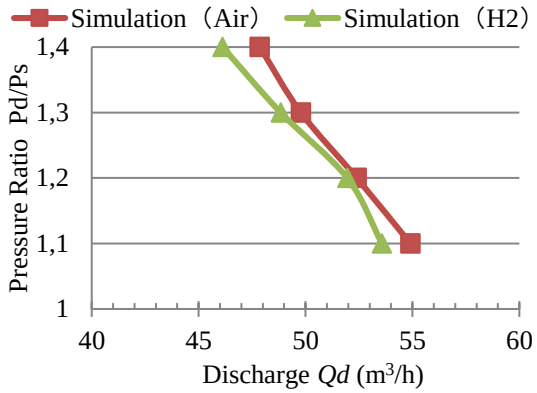

Fig. 6 Hydrogen circulating pump flow characteristics

4.2. Test system construction and experimental verification

To build the test system, to accurately measure the flow rate of the HCP, flow sensors are installed at the inlet and outlet. The processdiagram and physical picture are shown in Figs. 7 and 8. The control valve at the end is used to adjust the outlet pressure of the hydrogen pump, to measure the corresponding relationship between the flow rate and the pressure ratio. Considering that hydrogen is a flammable and combustible gas in the environment, air medium is used for performing experiments.

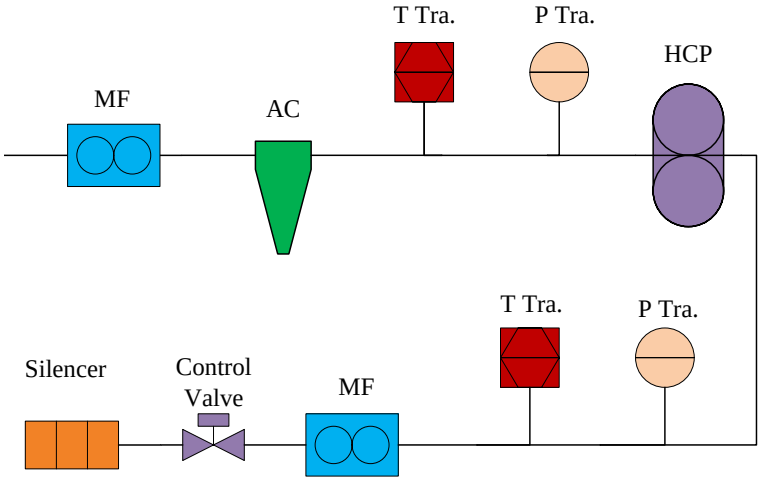

Fig. 7 Test system process diagram

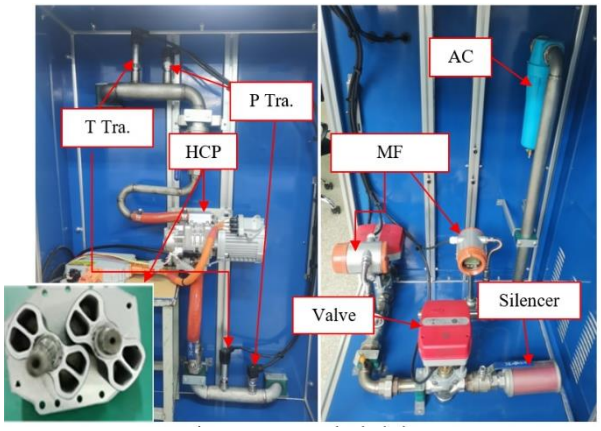

Fig. 8 Test system physical picture

The comparison between the simulation calculation and experimental results of the hydrogen circulating pump model in the air medium is shown in Fig. 9. It is found that the simulated Q_d of the same pressure ratio is greater than the experimental value. As the pressure ratio increases, the error between the two values increases from small to large. The error under the 1.1 pressure ratio is 3.6 % and grows to 10.0 % under the 1.4 pressure ratio. Analyzing the phenomenon that the error becomes larger, it is found that compared with the adiabatic boundary set in the simulation, the temperature of the pump body increases significantly with the increase of the pressure ratio during the experiment. At the 1.1 pressure ratio, the pump body temperature is 296 K and rises to 360 K at the 1.3 pressure ratio. Set the simulated adiabatic boundary temperature to 360 K, and obtain an error of 3.88 % at the pressure ratio of 1.3. It can be seen that when the pressure ratio is high, the high temperature of the pump body causes the volume of the intake air to expand, resulting in a smaller standard volume flow rate at the outlet. Therefore, the simulation calculation under the low-pressure ratio can directly replace the experimental research work and needs to consider the influence of temperature rise under the high-pressure ratio.

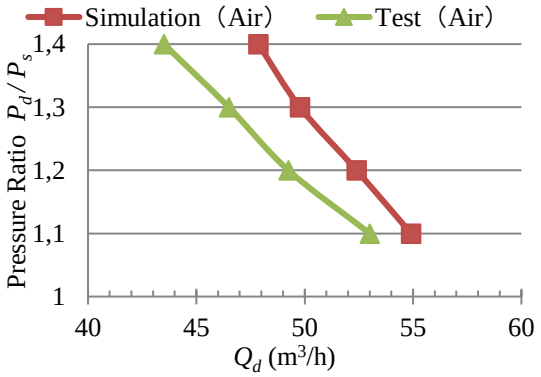

Fig. 9 Comparison of experimental and simulation data

5. Performance analysis of different rotor profiles

5.1. Profile shape

The fluid characteristics corresponding to the rotor profiles of various shapes are also distinct for the hydrogen circulating pump. To analyze the difference and obtain arotor profile with better fluid characteristics, three new rotor profiles have been designed according to the profile design method, and the conditions are given above. The curves *I* of the three profiles are single-arc, ellipse, and quadratic-curve, respectively. For the convenience of description, the rotor designed according to the two-tangent-arcs above is denoted as 1# rotor. The current rotors designed according to single-arc, ellipse, and quadratic-curve are designated as 2#, 3#, and 4# rotors, respectively. The formula of the curve *I* for 2# rotor is:

$$\begin{cases} \boldsymbol{L}_1 = \begin{bmatrix} b + r\cos t \\ r\sin t \\ 1 \end{bmatrix} \quad \left(0 \le t \le \pi - \arcsin\left(\frac{R\sin\alpha}{r}\right)\right) \\ b = \dfrac{R_m^2 - R^2}{2R_m - 2R\cos\alpha} \\ r = R_m - b \end{cases} . \quad (15)$$

The formula of the curve *I* for the 3# rotor is:

$$\begin{cases} \boldsymbol{L}_1 = \begin{bmatrix} x_0 + k_1\cos t \\ k_2\sin t \\ 1 \end{bmatrix} \quad \left(0 \le t \le \arcsin\left(\frac{R\sin\alpha}{k_2}\right)\right) \\ k_1 = R_m - x_0 \\ k_2 = \dfrac{R\sin\alpha}{\sqrt{1 - \left(\dfrac{R\cos\alpha - x_0}{k_1}\right)^2}} \\ x_0 = 5 \quad (x_0 \text{ is a parameter with adjustable value}) \end{cases} . \quad (16)$$

The formula of the curve *I* for the 4# rotor is:

$$\begin{cases} \boldsymbol{L}_1 = \begin{bmatrix} R_m - kt^2 \\ t \\ 1 \end{bmatrix} \quad \left(0 \le t \le R\sin\alpha\right) \\ k = \dfrac{R_m - R\cos\alpha}{R^2\sin^2\alpha} \end{cases} . \quad (17)$$

Substitute the corresponding $\boldsymbol{L}_1$ of the 2#, 3#, and 4# rotors into the formula (11), and then complete the formula calculation and graph drawing according to the corresponding relationship of the parameters in the formula (8). The structure and shape comparisons of the four profiles are shown in Fig. 10.

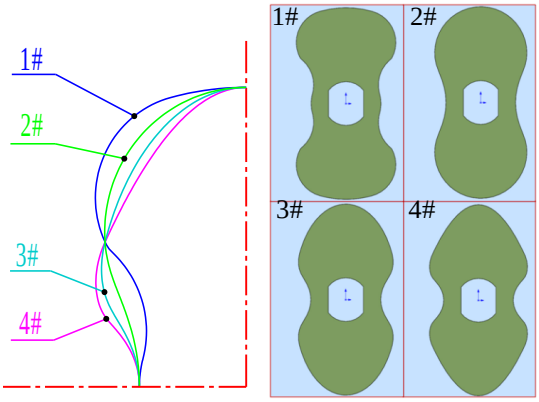

Fig. 10 Comparison of four-rotor profiles

5.2. Theoretical flow

The HCP models corresponding to 1#, 2#, 3#, and 4# rotors are called 1#, 2#, 3#, and 4# models, respectively. Calculate the displacement of the four models, and calculate the theoretical flow according to the rotation speed of 6000rpm. The results are shown in Table 2. According to the calculation results, the theoretical flow rate of the 1# model to the 4# model increases in turn. The smallest 1# model is 70.0 m³/h, and the largest 4# model is 74.7 m³/h.

5.3. Simulation results

Set the fluid medium as hydrogen, the running speed as 6000 rpm, and the pressure ratio P_d/P_s as 1. The simulation is performed according to the previous simulation calculation method, and the obtained flow characteristics are shown in Fig. 11.

Table 2

Theoretical flow comparison

Model No.	Cross-sectional area of a single rotor, mm^2	Displacement, mL/r	Theoretical flow rate m^3/h
1#	1781	194.3	70.0
2#	1734	200.0	72.0
3#	1698	204.3	73.5
4#	1672	207.4	74.7

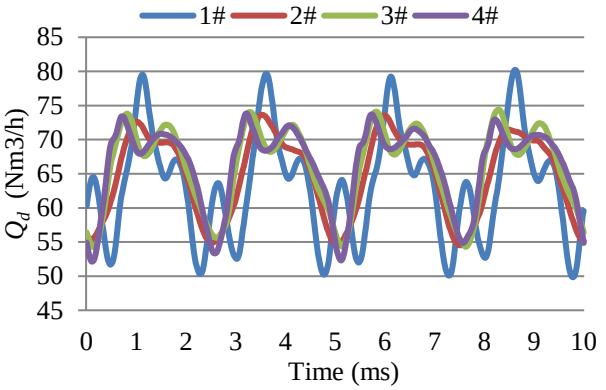

Fig. 11 Comparison of flow characteristics of four models

From the analysis of the flow waveform, the HCP model runs one cycle in 10ms, forming four flow fluctuation periods. The 1# model has the fluctuation range and the most complex waveform. The fluctuation of the 2# model is relatively stable, and the flow waveform is the simplest. The flow waveforms of the 3# and 4# models are similar, and the amplitudes are roughly the same.

Calculate the average flow rate Q_d of the four models according to the flow waveform, and get the value of the 1# rotor is 63.16 Nm^3/h, of the 2# model is 64.76 Nm^3/h, of the 3# model is 66.07 Nm^3/h, and of the 4# model is 66.34 Nm^3/h. It can be found that the simulated Q_d of the 1# to 4# models increases in turn, which is the same as the theoretical flow rate, and each simulation value is approximately 90% of the theoretical value.

To analyze the change of pressure distribution and velocity distribution inside the pump chamber during the rotor operation, one fluctuation period is divided into 6 states, with the adjacent angle being18º, as shown in Figs. 12 and 13.

Analyze the pressure changes of the four models in a flow fluctuation period. For 1# model, the maximum pressure is 476 Pa at 90º, the minimum pressure is 189 Pa at 54º; for 2# model the maximum pressure is 235 Pa at 18º, the minimum pressure is 57.3 Pa at 72º; for 3# model, the maximum pressure is 637 Pa at 0º, the minimum pressure is 26 Pa at 36º; for 4# model, the maximum pressure is 1570 Pa at 90º, and the minimum pressure is 57.6 Pa at 36º. It can be seen that the 2# model has the smallest pressure pulsation, the 4# model has the largest, the 1# model and the 3# model are in the middle level, and the 1# model is slightly better than the 3# model. The maximum pressure of the four models in the six states is generally located at the outlet of the contact between the two rotors, and the minimum value is generally located at the inlet of the contact between the two rotors.

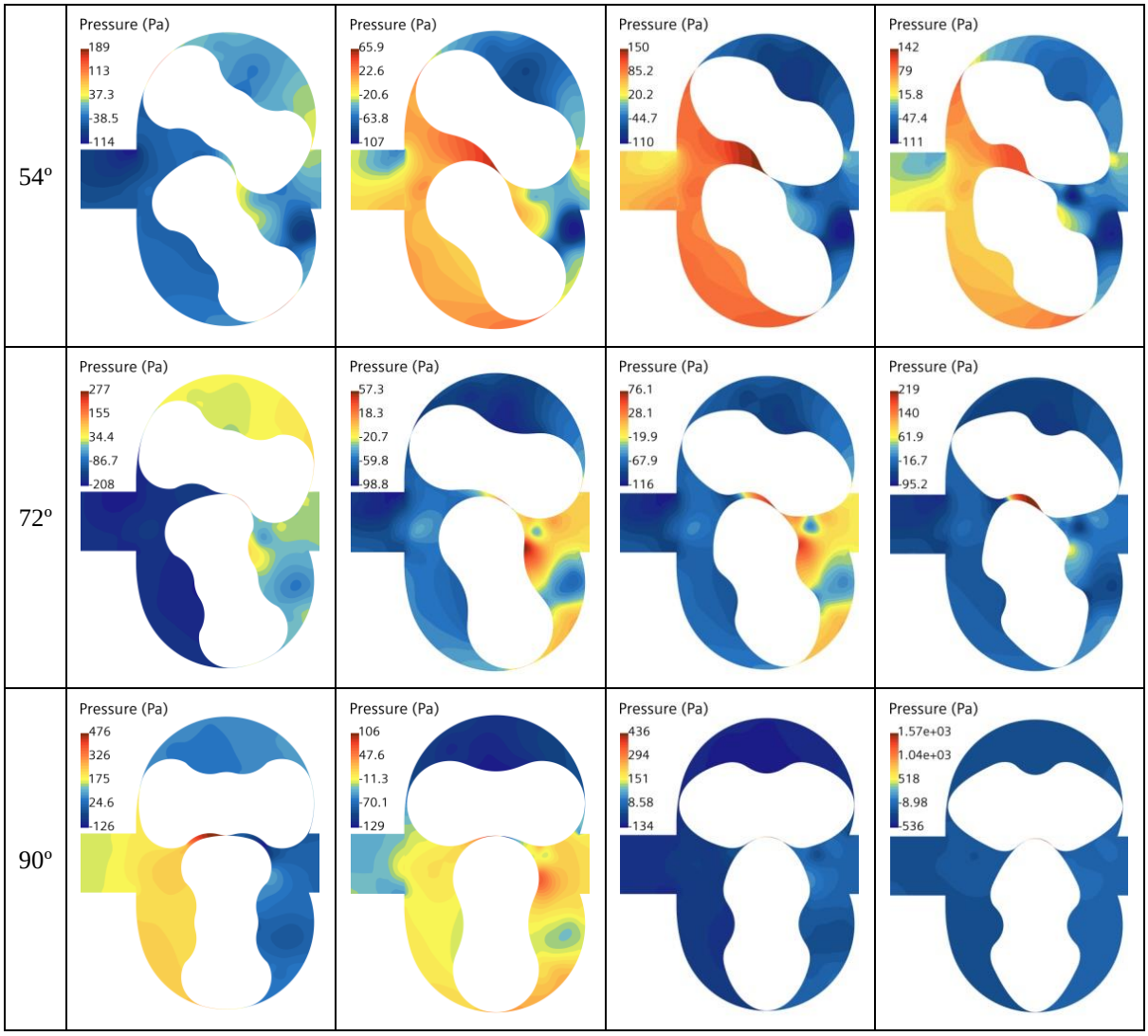

Fig. 12 Pressure distribution changes for the four models

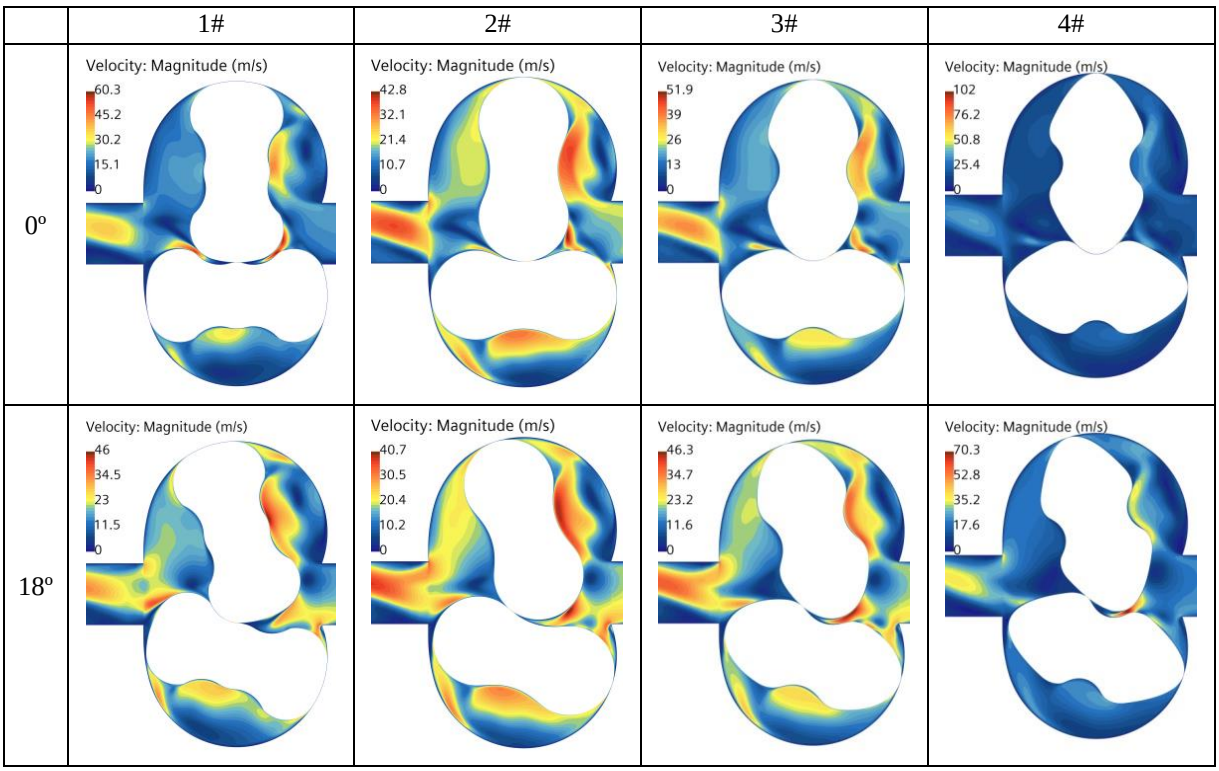

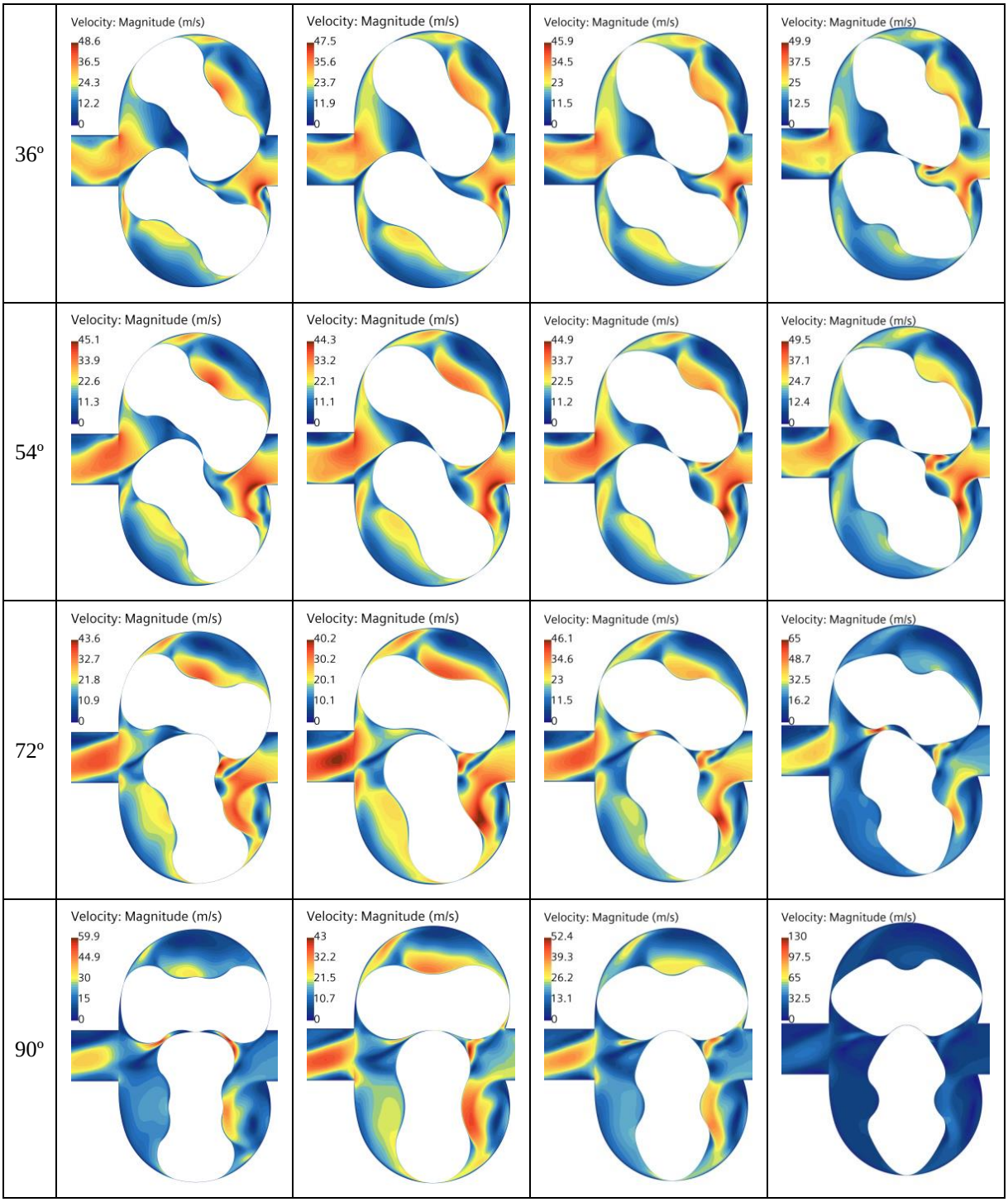

Fig. 13 Velocity distribution changes for the four models

Analyze the velocity changes of the four models in a flow fluctuation period. The velocity pulsation and the average velocity of the 2# model are both the smallest, with the maximum velocity at the state of 36º.The two values of the 4# model are both the largest, with significantly higher flow velocity at the two states of 0º and 90º.Similarly, the situation of the 1# model and the 3# model is in the middle level, but the 3# model is better than the 1# model. Both models have relatively high flow rates at 0º and 90º.The flow rates of the four models at 36º and 54º differ very little.

Based on the above comparison, it can be seen that the 1# model is not the best choice because the average flow rate is the smallest, the flow rate pulsation is the largest, and the pressure pulsation and flow rate pulsation are not optimal. Although the 4# model's average flow rate is the largest, its pressure pulsation and flow rate pulsation are significantly higher than those of the other three models, resulting in the worst flow stability, so the 4# rotor profile is also not the best choice. Analyze the 2# model and the 3# model, which have their advantages in terms of average flow and flow stability. The advantage of the 3# model in average flow rate is small, but the disadvantages in pressure pulsation, flow waveform, and flow velocity pulsation are larger. So it is judged that the 2# rotor profile is the best choice, and the 3# rotor profile is the second.

6. Conclusion

This paper proposes a general design method for the rotor profile of the hydrogen circulating pump, compares the data difference between air medium and hydrogen medium, and experiments using two-tangent-arcs rotor. Finally, the fluid characteristics of four types of rotors are analyzed, and the optimal profile is determined.

1. According to the conjugation principle, the general formula for the rotor profile design of the hydrogen circulating pump is summarized, which can be used to design the rotor profile of various shapes.

2. Using the overset mesh method and the realizable k-epsilon two-layer turbulence model to simulate the fluid characteristics of the hydrogen circulating pump, the average volume flow error of hydrogen medium and air medium is small. Compared with the experiment, this simulation method has high reliability at a low-pressure ratio. The influence of ambient temperature needs to be considered at a high-pressure ratio.

3.Evaluating the average flow rate and flow stability of four types of rotors, including two-tangent-arcs, single-arc, ellipse, and quadratic-curve, it is found that the overall performance of the single-arc rotor is the best, followed by the elliptical arc rotor, the quadratic-curve rotor has the largestaverage flow but the worst flow stability, and the two-tangent-arcs rotor has the smallest average flow.

References

1. **Lixin Fan; Zhengkai Tu; Siew Hwa Chan.** 2021. Recent development of hydrogen and fuel cell technologies: A review. Energy Reports,7. https://doi.org/10.1016/j.egyr.2021.08.003.
2. **Abdul Alami Hai.** 2020. Developments of hydrogen fuel cell technologies, International Journal of Hydrogen Energy. https://doi.org/10.1016/j.ijhydene.2020.12.039.
3. **Falin Chen; Yu-Guang Su; Chyi-Yeou Soong;** et al. 2004, Transient behavior of water transport in the membrane of a PEM fuel cell, Journal of Electroanalytical Chemistry 566(1):85-93. https://doi.org/10.1016/j.jelechem.2003.11.016.
4. **Cui, D. Z.; Xiao, J. S.; Pan, M.; Yuan, R. Z.** 2005. Water, heat and gas management of proton exchange membrane fuel cell, Battery Bimonthly 34(5):373-375.
5. **Promislow, K.; St-Pierre, J.; Wetton, B.** 2011. A simple, analytic model of polymer electrolyte membrane fuel cell anode recirculation at operating power including nitrogen crossover, Journal of Power Sources 196(23): 10050-10056. https://doi.org/10.1016/j.jpowsour.2011.08.070.
6. **Wilhelm Wiebe; Thomas von Unwerth; Sven Schmitz.** 2020. Hydrogen pump for hydrogen recirculation in fuel cell vehicles, E3S Web of Conferences 155.
7. **Feng, J.; Han, J.; Hou, T.; Peng, X.** 2020. Performance analysis and parametric studies on the primary nozzle of ejectors in proton exchange membrane fuel cell systems, Energy Sources Part A Recover. Util. Environ. Eff.
8. **Ma Qiuyu; Wang Yupeng; Du Jing; Huang Xing.** 2019. Research on the hydrogen circulation system of fuel cell, Hydrogen Fuel Cell Vehicle Technology 4: 11-14.
9. **Wang, J.; Jiang, X.; Cai, Y.** 2015. Investigation of a novel circular arc claw rotor profile for claw vacuum pumps and its performance analysis, Vacuum 111: 102–109. https://doi.org/10.1016/j.vacuum.2014.10.003.
10. **Gu Pengtai; Xing Linfen;** et al. 2020. Transient flow field and performance analysis of a claw pump for FCVs, International Journal of Hydrogen Energy. https://doi.org/10.1016/j.ijhydene.2020.09.154.
11. **Zhang, Q.; Feng, J.; Wen, J.; Peng, X.** 2018. 3D transient CFD modeling of a scroll-type hydrogen pump used in FCVs, International Journal of Hydrogen Energy 43: 19231–19241. https://doi.org/10.1016/j.ijhydene.2018.08.158.
12. **Qingqing Zhang; Jianmei Feng;** et al. 2019. Performance prediction and evaluation of the scroll-type hydrogen pump for FCVs based on CFD–Taguchi method, International Journal of Hydrogen Energy 44(29): 15333–15343. https://doi.org/10.1016/j.ijhydene.2019.04.019.
13. **Simon, E.; Tian, G.; John, C.** 2018. A review of scroll expander geometries and their performance, Appl. Therm. Eng. 141: 1020e34. https://doi.org/10.1016/j.applthermaleng.2018.06.045.
14. **Wang Yupeng; Ma Qiuyu; et al.** 2019. Fuel cell engine technology overview, Fuel Cell Vehicle Technologies 01: 42-47.
15. **Feng Jianmei; Xing Linfen; et al**. 2020. Effects of Working Fluids on the Performance of a Roots Pump for Hydrogen Recirculation in a PEM Fuel Cell System, Applied sciences-basel10(22).
16. **Jiawei Lin; Lixin Zhang;** et al. 2021. Rotor profile design and motion simulation analysis of hydrogen circulating pump, International Journal of Fluid Machinery and Systems 14(4).
17. **Xing Linfen; Feng Jianmei;** et al. 2020. Development and testing of a roots pump for hydrogen recirculation in fuel cell system, Applied sciences-basel 10(22).
18. **Liu Linlin; Chen Peijun; Du Jinqiao; Wang Xinyi.** 2020. Study on involute rotor profile based on pressure angle reduction, Journal of Physics: Conference Series 1550(4).
19. **Xu Wen-bin; YU Zhen-hua; HU Huan-lin.** 2006. Study on the profile of eccentric-arc-shaped root rotor. Fluid Machinery (04): 41-43.
20. **Shen Hao; JIa Kun ;** et al. 2014. Optimization design of cam pump rotor profile and simulation of pump performance, Journal of Lanzhou University of Technology 03: 44-48.
21. **Zhang Tiezhu; Zhang Hongxin; Zhao Hong.** 2002. Theoretical and practical design of un-contact rotor pump profile, Chinese Journal of Mechanical Engineering 38(11): 152-155.
22. **Zhang Hongxin; Zhang Tiezhu; Zhang Jizhong; Yang Jianmin.** 2005.Optimization design of un-contact rotor pump, Transactions of the Chinese Society of Agricultural Machine 36(7): 65-67.
23. **Sung-Yuen Jung; Jun-Ho Bae; Moon-Saeng Kim; Chul Kim.** 2011. Development of a new gerotor for oil pumps with multiple profiles, International Journal of Precision Engineering and Manufacturing 12(5).
24. **Chiu-Fan; Hsieh.** 2015. A new curve for application to the rotor profile of rotary lobe pumps, Mechanism and Machine Theory 87. https://doi.org/10.1016/j.mechmachtheory.2014.12.018.

25. **Yan Jia, Daniel C. H. Yang; Tong Shih-Hsi.** 2009. A new gerotor design method with switch angle assignability, Journal of Mechanical Design 131(1).
26. **Rodi, W.** 1991. Experience with two-layer models combining the k-epsilon model with a one-equation model near the wall, 29th AIAA Aerospace Sciences Meeting.

H. Zhai, W. Li, L. Ji, M. Awais, J. LI, S. Li

PROFILE DESIGN AND PERFORMANCE RESEARCH OF HYDROGEN CIRCULATION PUMP IN FUEL CELL SYSTEM

S u m m a r y

A general design formula for rotor profile is proposed based on conjugation theory and feasibly verified by using the four different design shapes. The overset mesh method and the realizable k-ε two-layer turbulence model are used for simulation calculation. The results stated that the average volume flow error of hydrogen medium and air medium is small, so an alternative experimental study has been carried out. By building a test system for experimental verification, it is found that the error between the simulation results and the experimental results is small at the low-pressure ratio and increases at the high-pressure ratio because the influence of the ambient temperature is not considered. The results further verified the reliability using the simulation calculation method. At last, the fluid characteristics of the two-tangent-arcs type, single-arc type, ellipse type, and quadratic-curve type rotors are evaluated. The result shows that the comprehensive performance of the single-arc type rotor is superlative as followed by the ellipse type rotor. However, the quadratic-curve rotor has the largest average flow but the worst flow stability and the two-tangent-arcs rotor shows the smallest average flow.

Keywords: fuel cell system, hydrogen circulation pump (HCP), profile design, overset mesh, CFD.

Received May 31, 2022
Accepted August 24, 2022

This article is an Open Access article distributed under the terms and conditions of the Creative Commons Attribution 4.0 (CC BY 4.0) License (http://creativecommons.org/licenses/by/4.0/).